Oxidation of Metals (2021) 95:251–268
https://doi.org/10.1007/s11085-021-10022-1

ORIGINAL PAPER

High Temperature Oxidation and Decarburization of *SiMo* Cast Iron in Air and Combustion Atmospheres

Simon N. Lekakh[1] · Asebi Bofah[1] · Richard Osei[1] · Ron O'Malley[1] · Larry Godlewski[2] · Mei Li[2]

Received: 23 September 2020 / Revised: 4 January 2021 / Accepted: 11 January 2021 /
Published online: 2 April 2021

Abstract

Silicon and molybdenum (*SiMo*) alloyed cast irons with spherical graphite are used for exhaust manifolds for service at high temperatures in air and combustion atmospheres containing water vapor. Analysis of degraded surfaces of in-service manifolds indicates existence of a combined oxidation and de-carburization (de-*C*) phenomena. Therefore, sequential high-temperature tests in air and combustion atmosphere with recording weight change together with carbon analysis at each time step were utilized to quantify the kinetics of both processes. The recorded weight change was related to weight gain due to oxidation and weight loss due to de-*C*. Carbon analysis was used to de-couple these two processes. SEM measured thicknesses of de-*C* layers were used to verify kinetics obtained from changes in carbon concentration during oxidation. It was shown that the oxidation and de-*C* kinetics have different sensitivities to testing temperature and the type of oxidizing atmospheres. At 700 °C and above, there are several significant mutual effects between scale formation and de-*C* processes which affect the kinetics of these processes and activation energy. The tested experimental methodology for decoupling these processes can be used for alloy optimization.

Keywords *SiMo* cast iron · Oxidation · De-carburization · Scale structure · Kinetics

Introduction

In order to meet future emission regulations and improve fuel efficiency, the temperature of the exhaust gases in automotive engines is projected to increase [1]. Therefore, the need exists to improve cast materials which could combine exceptional

✉ Simon N. Lekakh
lekakhs@mst.edu

[1] Missouri University of Science and Technology, Rolla, MO 65409, USA

[2] Research and Innovation Center, Ford Motor Company, Dearborn, MI 48124, USA

technological properties, such as low solidification shrinkage and high fluidity needed to cast complicated shape thin wall manifold, with possibility to operate at higher temperatures in an oxidizing atmosphere. Cast irons with spherical graphite that are highly alloyed with silicon and molybdenum (*SiMo*), and sometimes with chromium and aluminum additions, have been proposed for use in cast exhaust manifolds to increase the oxidation resistance [1–5]. During high temperature exposure of *SiMo* cast iron in air and contained water vapor exhaust gases, a multi-layered oxide scale is formed. This scale consists of outer layers of hematite and magnetite growing outward, an inner layer of magnetite and spinel phases growing into the substrate, and a thin barrier film of SiO_2 (silica) at the oxide/metal interface [5–8]. In addition, a deeply de-carburized (de-*C*) layer in the matrix has been observed [5]. It was found that oxidation of these alloys in exhaust gases is more extensive than in air because the protective silica film is less effective in the presence of a water vapor containing environment [9, 10]. The protective role of the silicon-rich oxide film at metal-oxide interface has also been investigated and the thickness and continuity of silica is proposed to control both the oxidation and de-*C* kinetics. In humid exhaust gases, the silica film is not always continuous, which could be due to the several processes, including: an increase in oxygen permeability in iron with water vapor and de-*C* of the metal matrix. Therefore, a coupled analysis of the kinetics of oxidation and the de-*C* processes is important because both processes occur simultaneously during surface degradation of *SiMo* ductile iron.

De-*C* and scale formation of iron alloys both play an important role in many metallurgical processes, as well as during service life. In most cases, de-*C* is considered to have a negative impact on product quality and the metallic component integrity during service. Therefore, attempts are made to avoid or minimize de-*C* during continuous casting, slab re-heating for hot rolling, and in different heat treatment operations of steel and cast irons. De-*C* of iron-carbon alloys can be a serious problem because the degraded surface layer reduces strength, wear resistance, and can enable fatigue failures. Typically, during metallurgical processes, scale formation and de-*C* occur simultaneously [11]. The de-*C* behavior of high carbon 60Si2MnA steel in dry and wet atmospheres containing different amounts of O_2 with or without CO_2, at 700–1000 °C has been investigated [12, 13]. It was observed that severe de-*C* was associated with the formation of wustite (*FeO*) scale and the de-*C* tendency at 800 °C was greater than at 700 °C or 900 °C. When *FeO* was suppressed by heating in dry O_2 containing gases, surface de-*C* was inhibited by a silica film. At a higher temperature (1000 °C), *FeO* was able to form on the austenite matrix, and de-*C* tendency was alleviated because of lower carbon diffusivity in austenite compared with in ferrite. According to [13], samples treated at 700 °C in the ambient air showed measurable de-*C* layer. In the presence of water vapor, no de-*C* layer was observed and in contrast, intensive de-*C* process was observed in completely dry air. To analyze oxidation and de-*C* kinetics separately, the measured apparent weight gains after the test was adjusted by weight loss due de-*C*. The weight loss was calculated from the measured thickness of the de-*C* layer.

However, de-*C* of iron-carbon alloys can be specifically designed as tool for solid state steel production [14–16]. In these processes, supplemental oxidation tried was suppressed and avoided by carefully controlling temperature and

surrounding environment. The solid-state de-*C* is considered to be an effective way to transform high-carbon cast iron into low-carbon steel with minimal environmental impact. Controlled solid-state de-*C* was also suggested to develop functional gradient materials, such as multi layered sheet production with a ductile low-carbon external layer and a high-strength high carbon core [17]. The controlled de-*C* process of cast irons was suggested for making a new engineering material [18]. In this process, pores from de-*C* subsurface graphite particles were infiltrated by alternative materials. The effects of holding time, temperature, and chemical composition were investigated for different graphite morphologies (flake graphite, compacted graphite, and spheroidal graphite). The rate of formation of surface porosity was faster in flake graphite irons than that for the other graphite morphologies. It happened because flake graphite is interconnected phase in the matrix, whereas graphite nodules are separated from each other.

The authors recently performed qualitative non-destructive μCT and SEM/EDX analysis of oxidized high *SiMo* cast iron in air and in synthetic combustion atmospheres at 700 °C and 800 °C [19]. Figure 1 illustrates a degraded surface of *SiMo* ductile iron consisting of an external iron oxide, an internal layer of mixed *Fe-Si* oxides, a thin silica film, and a de-*C* layer that extended into the metal matrix with spherical pores from oxidized graphite nodules (Fig. 1a). It was shown that increasing the test temperature and water vapor in combustion atmosphere both change scale morphology from a uniform layer growth to highly nonuniform layer. An example of 3D shape of nonuniform oxide layer is shown Fig. 1b. The transformation of uniform to nonuniform scale structures was linked to the intensity of the de-*C* process, while kinetics of these reactions in *SiMo* cast iron was not quantified. Surface degradation during oxidation and thermomechanical load plays important role in fatigue crack initiation [20] and qualitative analysis of these processes is important for manifold lifetime prediction.

The objective of this study was quantitative characterization of both oxidation and de-C processes during exposing SiMo cast iron on air and combustion gas atmosphere at different temperatures.

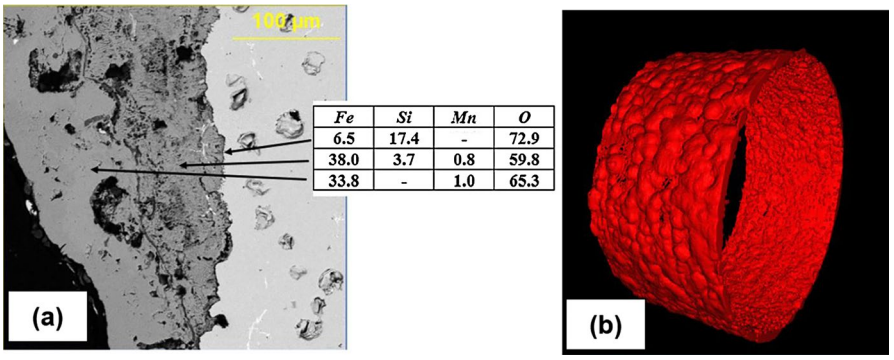

Fig. 1 *SiMo* cast iron oxidized in air at 800 °C during 100 h: (**a**) SEM/EDX analysis of multilayered scale structure and (**b**) μ-CT scan of the nonuniform scale layer [19]

Table 1 Chemistry of *SiMo* cast iron (wt%)

C	*Si*	*Mn*	*Mo*	*Ni*	*Cr*	*Mg*	*P*
3.20	4.25	0.34	0.71	0.20	0.05	0.03	0.02

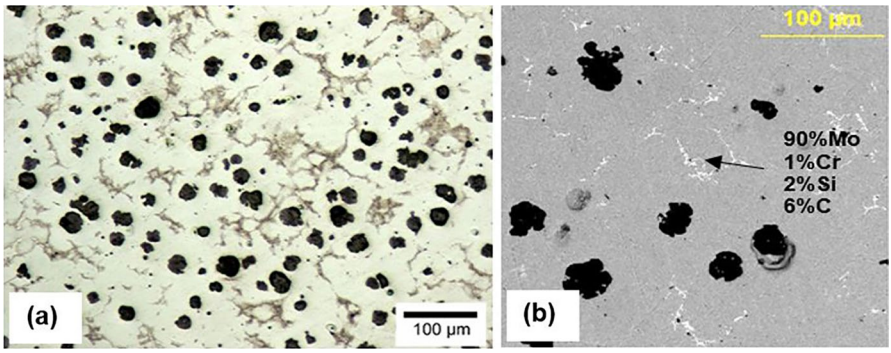

Fig. 2 Optical microstructure (**a**) and SEM/EDX analysis (**b**) of *SiMo* cast iron. Graphite nodules are black and complex *Mo*-carbides locate at grain boundaries are bright on SEM image

Procedures

Investigation of Surface Structure of In-Service Manifolds

This analysis was performed to verify surface degradation of car manifolds after 97,000 miles service. There were no indicators of macro-cracks or other large defects which could require decommissioning of the manifolds. The specimens were extracted from the manifold using core drilling, and they were studied using SEM/EDX Aspex system and Raman spectroscopy in cross sections from both surfaces: the internal surface exposed to combustion gases (exhaust surface) and the external surface oxidized in air (air surface). This manifold was made from *SiMo* cast iron with a composition similar to the composition used in the main study presented in this article (Table 1).

Experimental

The chemistry of the studied *SiMo* cast iron, measured by spectral analysis (main elements) and Leco combustion (*C*), is given in Table 1. This alloy contained 3.2% *C* (to form graphite eutectic), 4.2% *Si* (for oxidation protection), 0.7% *Mo* (for creep resistance), and 0.03% *Mg* (for graphite phase spheroidization). Optical and SEM images of studied alloy are given in Fig. 2. The structure in the as-cast condition consisted of near spherical graphite nodules distributed in silicon alloyed ferritic matrix and complex molybdenum carbide, which are located at

the grain boundaries. High *Si* alloying has adverse effect on the shape of graphite nodules in *Mg*-treated cast iron and decreases it nodularity index [21].

The used *SiMo* cast iron had 3.2% *C*; therefore, de-*C* could occur simultaneously with oxidation during high-temperature exposure in air or in exhaust gases. To study both processes, the procedure included recording changes in weigh (ΔG_{ex}) and carbon concentration (ΔC, wt%) using multiple specimens, one for each specific test time. The tests were performed using rectangular-shape specimens that measured $4 \times 12 \times 35$ mm, which were milled from a cast plate and subjected to wet grinding with 60 grit silicon carbide wheel on all sides of the specimens. Two experimental sets were performed. In the first experimental set, the oxidation tests were performed to study reaction kinetics in combustion atmosphere. These tests were performed with several sequential time steps up to 200 h at 700 °C, 750 °C, and 800 °C. One specimen was removed from furnace after cooling in controlled atmosphere after each time step. The remained specimens were again heated to continue oxidation test. In the second comparison set, tests were performed on air and combustion atmosphere without interruption during 100 h at 650 °C, 700 °C, 750 °C, and 800 °C. This temperature range is considered a normal upper working temperature range for exhaust automotive components made from *SiMo* cast iron. In both sets, oxidation was performed in a preliminary treated at 1000 °C open shallow rectangular shaped alumina crucible. The shape of the crucible permitted gas flow around all specimen surfaces and collect spalled scale.

A three-channel mass flow meter was used to prepare the synthetic combustion atmosphere, which consisted of 2 vol% O_2, 15 vol% CO_2, and remaining N_2. The applied 500 ml/min gas mixture flow rate was sufficient to prevent gas starvation due to specimen oxidation in the furnace. An oxygen meter was used to check oxygen concentration in the furnace before and after testing. Water vapor equilibrium saturation (15 vol%) was performed by bubbling a gas mixture through a 500 ml volume water bath inside a heated stainless steel cylinder. An average humidity was also determined by recalculation from weight of water loss over the duration of the test. Two-zone sealed horizontal quartz tube furnace was used at ambient pressure for these tests with ± 1 °C precision of temperature control. The furnace tube was flushed for 30 min with combustion gas before and after each heating cycle.

Specimens and crucibles were weighed before and after experiments to determine a total "apparent" weight change per specimen unit area (ΔG_{exp}, g/m^2). After that, a central part of the specimen was sectioned in the transverse direction using a precision water cooled saw to extract a thin sample for Leco CS 500 combustion carbon analysis. This sample included the complete perimeter that was exposed to the oxidizing atmosphere during the test. A measured change in *C* concentration before and after the test (ΔC, wt%) was used to calculate weight loss due to de-*C* (ΔG_C), considering weight (*W,* g) and surface area (*S,* m^2) of a specimen: $\Delta G_C = 0.01 * \Delta C * W/S$. The shape and dimensions of the specimen were chosen to provide sensitivity of carbon analysis from surface de-*C* while prevent full de-*C* near the center. The "true oxidation" which presented an amount of oxygen reacted with metallic components to form scale ($\Delta G_{O\text{-scale}}$, g/m^2) was calculated from the measured weight gain (ΔG_{exp}) and adjusted by the weight loss due to de-*C* (ΔG_C). In addition, oxygen consumed for de-*C* ($\Delta G_{O\text{-}deC}$) was calculated from ΔG_C assuming the formation of *CO*

gas: $\Delta G_{O\text{-}deC} = (16/12)^{*}\Delta G_C$, g/m^2. To verify de-*C* measured from changing *C* concentration, an average thickness of the de-*C* layer was measured metallographically using SEM/EDX analysis with the ASPEX system. Using this measurement, the carbon loss (ΔG_C) was calculated from a measured thickness of de-*C* layer (micron), specimen total area and density, assuming zero carbon in ferritic matrix, a sharp boundary. Vice versa, a thickness of the de-C layer also was estimated from the Leco combustion test using similar assumption. The results of these two methods, from *C* analysis and SEM observation, were compared using the same de-*C* layer thickness parameter.

Thermodynamic Simulation

Prediction for competitive local oxidation reactions of active elements with the formation of multi-layered scale structures and de-*C* layer in *SiMo* cast iron was performed using FactSage 7.3 thermodynamic software [22]. The databases employed for the calculations included FSsteel, FToxid, and FactPS. The local equilibrium conditions were simulated by stepwise additions of oxygen into the alloy streams from the previous calculation step assuming irreversible reactions. The thermodynamic simulations were performed with the assumption that the local equilibrium condition was reached between the gas components, formed oxide phases, and the *SiMo* cast iron. This method allows one to predict different phases potentially formed at low (inner layer) and high (outer layer) oxygen partial pressure. Using a variety of oxygen/*SiMo* mass ratios, the different oxide phases which were formed under the local equilibrium condition were traced from low oxygen (for inner layer) to high oxygen ratios presented in the outer scale layer. The simulation temperature was 800 °C.

Results

In-Service Manifold Analysis

The significant differences in scale structure and chemistry between exhaust-side and air-side surfaces of in-service manifold were observed (Figs. 3, 4). Scale formed on the exhaust-side surface in contact with exhaust gases and had approximately 100 μm thickness (Fig. 3b). Internal porosity, cracks, and evidence of scale delamination were present. The mixed-wave layers in the exhaust-side scale had a combination of iron oxides and fayalite, with phosphorus and the other contaminations coming from combusted fuel (Table 2). This structure indicated partial renewal of surface layers because of scale cracking and spalling. Scale on the air-side surface was denser with fewer defects; however, the scale thickness was irregular and penetrated into a casting wall due to fatigue micro-crack propagation. Oxides were present in these cracks. In both cases, there was evidence of de-*C*, which was present as partially and completely empty "nests," which were previously occupied by graphite nodules (insert in Fig. 3c). The resultant round pores were incorporated

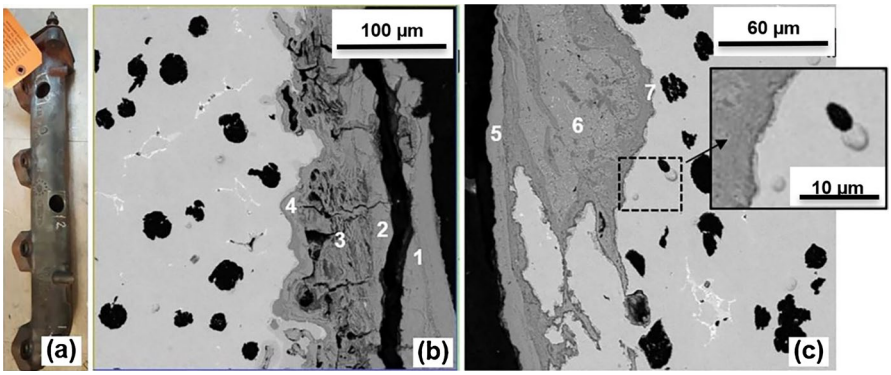

Fig. 3 Field car manifold with 97,000 miles servise (**a**) and cross section of surfaces near exhaust-side (**b**), and air-side (**c**)

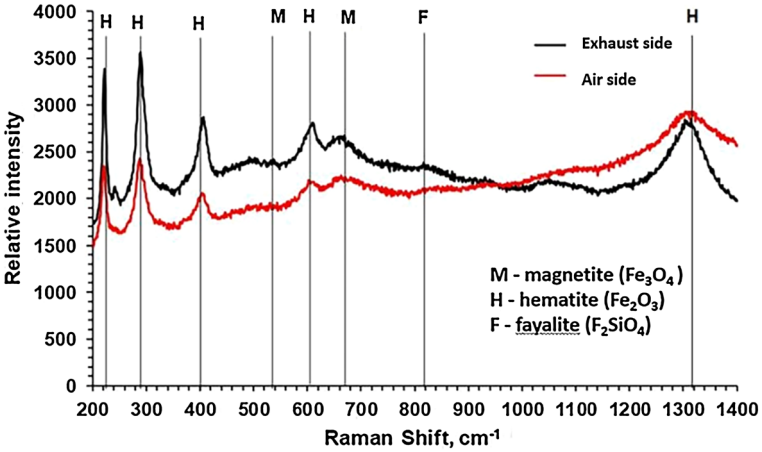

Fig. 4 Phases identified in scale of field manifolds using Raman spectroscopy

Table 2 EDX analysis (wt%) of phases in internal and external manifold surfaces (points from Fig. 3)

Point	*O*	*Fe*	*Si*	*Mn*	*Mo*	*P*
1	56	39	–	–	–	3.2
2	56	40	–	–	–	1.5
3	67	13	17.2		0.7	
4	59	34	4.9	0.5	–	1
5	54	46	–	0.4	–	1
6	53	40	3.9	0.8	0.6	–
7	20	70	5.5	1.1	–	–

into the scale structure and were also distributed along the boundary layer in the metal matrix at a 150–200 µm depth.

This observation demonstrated that coupled oxidation and de-*C* processes take place in the *SiMo* cast iron manifold during service. These processes are affected by time, temperature, atmosphere and thermo-cycling stress. The high compressive stresses in the exhaust manifold are caused by the high material temperature and restricted thermal expansion. When the stress exceeds the yield strength of the material, plastic deformation occurs and after the engine is cooled down, the compressive stress changes to local tensile stress. At different locations, compression stress promotes scale delamination from the casting wall, while tension stress initiates fatigue crack nucleation [23].

Oxidation Tests

The weight gain per unit area of the oxidized surface after sequential holding of five specimens for each test temperature (700 °C, 750 °C, and 800 °C) in a synthetic combustion atmosphere is shown in Fig. 5a. At lower test temperature (700 °C), the weight gain had a parabolic trend during the holding time, which is typical for a diffusion-controlled oxidation process. However, increasing the test temperature

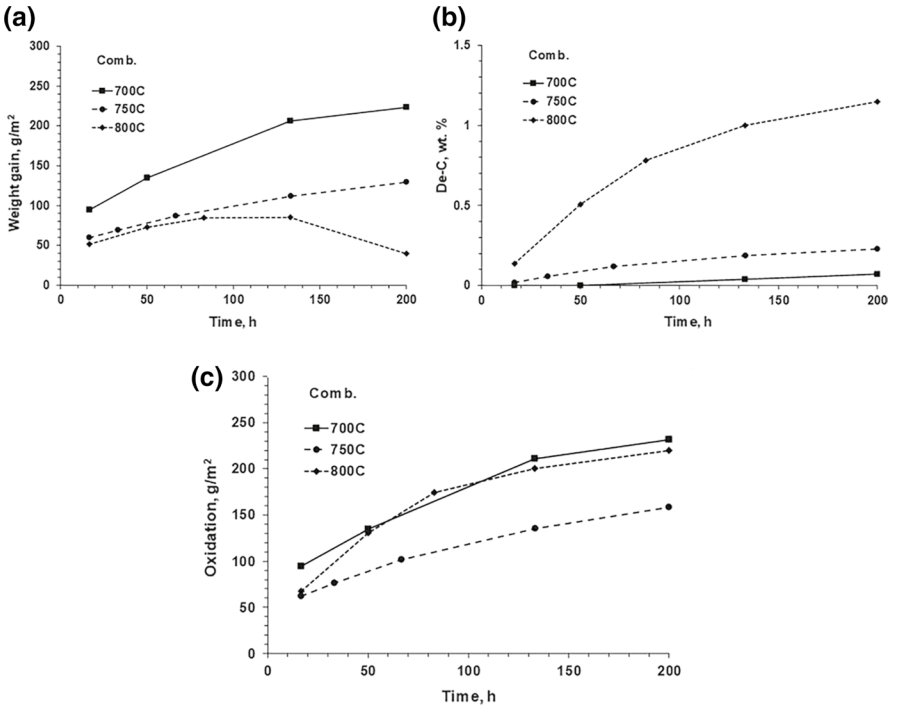

Fig. 5 Weight gain (**a**), carbon decrease due de-*C* (**b**), and calculated true oxidation (**c**) of *SiMo* cast iron tested in combustion atmosphere

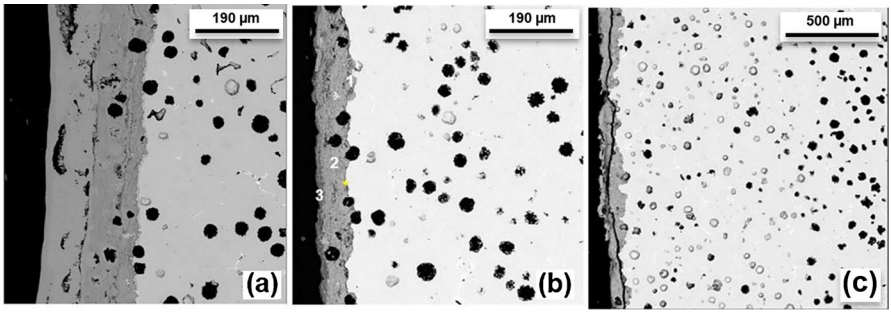

Fig. 6 Outer, inner and de-*C* layers in *SiMo* cast iron oxidized 200 h in combustion atmosphere at 700 °C (**a**), 750 °C (**b**) and 800 °C

Table 3 Local composition (wt%) of scale layers formed in *SiMo* cast iron oxidized during 200 h in combustion atmosphere at 750 °C (points from Fig. 6b)

Point	*O*	*Fe*	*Si*	*Mn*
1	46	41	9	1
2	58	34	3.7	1
3	59	35	1	–

to 750 °C changed the parabolic trend to a linear trend. A similar linear trend was observed during the initial oxidation period at 800 °C; however, weight gain decreased with increased test time. Such changes in weight gain were related to synergistic effects of the two nonlinear processes: weight gain due to oxidation with formation of oxide scale and weight loss due to de-*C*. A Leco combustion analysis of carbon concentration showed (Fig. 5b) that de-*C* was not significant in the specimens tested at 700 °C. However, the de-*C* rate increased at 750 °C test temperatures. The kinetic de-*C* curves exhibited a parabolic trend at high temperatures. Considering weight loss due to de-*C*, a true oxidation was calculated (Fig. 5c) from experimentally measured weight change (Fig. 5a).

All true oxidation curves had a parabolic trend but the oxidation rate did not increase proportionally with increasing the test temperature. Strong oxidation was observed at 700 °C with the formation of a thick and dense oxide layer (Fig. 6a). The oxidation rate declined with increasing the test temperature to 750 °C, which could be related to the intensified de-*C* process. At this temperature it was also found that the scale consisted of external iron oxides, an internal mixture of fayalite (Fe_2SiO_4) with iron oxide, and thin film of silica along the metal boundary (Fig. 6b and Table 3). Increasing the test temperature to 800 °C dramatically changed the scale topology. Cracks occurred parallel to the metal boundary in the internal layer and delamination of the external layer started at an early oxidation time (Fig. 6c). Due to the cracks, the scale spalling from the flat surface intensified with increasing exposure time.

In the second set, oxidation tests were performed at 100 h using four temperatures (650 °C, 700 °C, 750 °C, and 800 °C) in both the combustion atmosphere and in the air. This uninterrupted set of tests was performed to avoid additional stress on scale

during several cooling/heating cycles, which were applied in interrupted first test set. In the combustion atmosphere, the scale that formed at 650 °C was mostly dense throughout the external and internal layers with pockets of pores in the external scale layer. Like to observed in set 1 (Fig. 6), cracks in the external layer appeared at 700 °C, and active delamination was visible at 750 °C. In both, first and second sets, both scale layers (internal and external) had massive porosity and multiple cracks in specimens oxidized at 800 °C in the combustion atmosphere.

Samples oxidized in the air for 100 h exhibited less severe scale defects (Fig. 7) when compared with oxidation in the combustion atmosphere. Oxide layers were relatively dense at 650 °C and 700 °C and had uniform scale/metal boundary and scale thickness. Porosity in the external layer and uneven scale thickness and scale/metal interface were observed at the elevated temperature of 750 °C. Severe cracking and delamination of the external oxide layer was present at 800 °C (Fig. 7). Significant de-*C* layers were present in the specimens exposed to air at 750 °C and 800 °C.

Leco combustion analysis also showed that a decrease in carbon intensified at high temperatures (see De-*C* curve in Fig. 8). This carbon change was used to calculate weight loss due to de-*C*. Both, weight gain due to oxidation and weight loss due to de-*C* were used to calculate the true oxidation rate (see oxidation curve Fig. 8). The minimal true oxidation rate was observed at 700 °C and it increased with increasing temperature to 800 °C.

Discussion

Continuous and cycled heating/cooling thermo-gravimetric analysis (TGA) that monitors specimen weight change is a common method used to study high-temperature oxidation of metallic alloys. However, in *SiMo* cast iron case, TGA will record apparent weight change during oxidation, which is the results of several processes, including oxidation of metallic components (weight gain), as well as weight losses due to spalling scale and de-*C*. In these conditions, to obtain "true" oxidation of metallic alloy components, the measured apparent weight change during experiment needs to be adjusted by: (i) the amount of lost carbon and (ii) spalled scale. Therefore, to study reaction kinetics, experiments in set 1 were performed in several time steps with collecting spalled scale in crucible and using multiple specimens for followed carbon analysis. Also, experiments in additional set 2 were performed at 100 h to compare oxidation on air and combustion atmosphere contained water vapor. After each test, slice from a specimen middle section with whole oxidized perimeter was used for combustion carbon analysis. The thickness of used specimens was chosen to get a measurable carbon change and simultaneously avoid complete de-*C* of a middle part. This procedure was used to decouple surface oxidation of metallic component and surface scale formation from internal de-*C*.

Experiments showed that surface and subsurface degradation in *SiMo* cast iron with spherical graphite during service is related to the complex effect of oxidation and de-*C*. At 650 °C, oxidized surfaces did not show signs of de-*C*. However, these two processes occurred simultaneously at a higher oxidation temperature. It

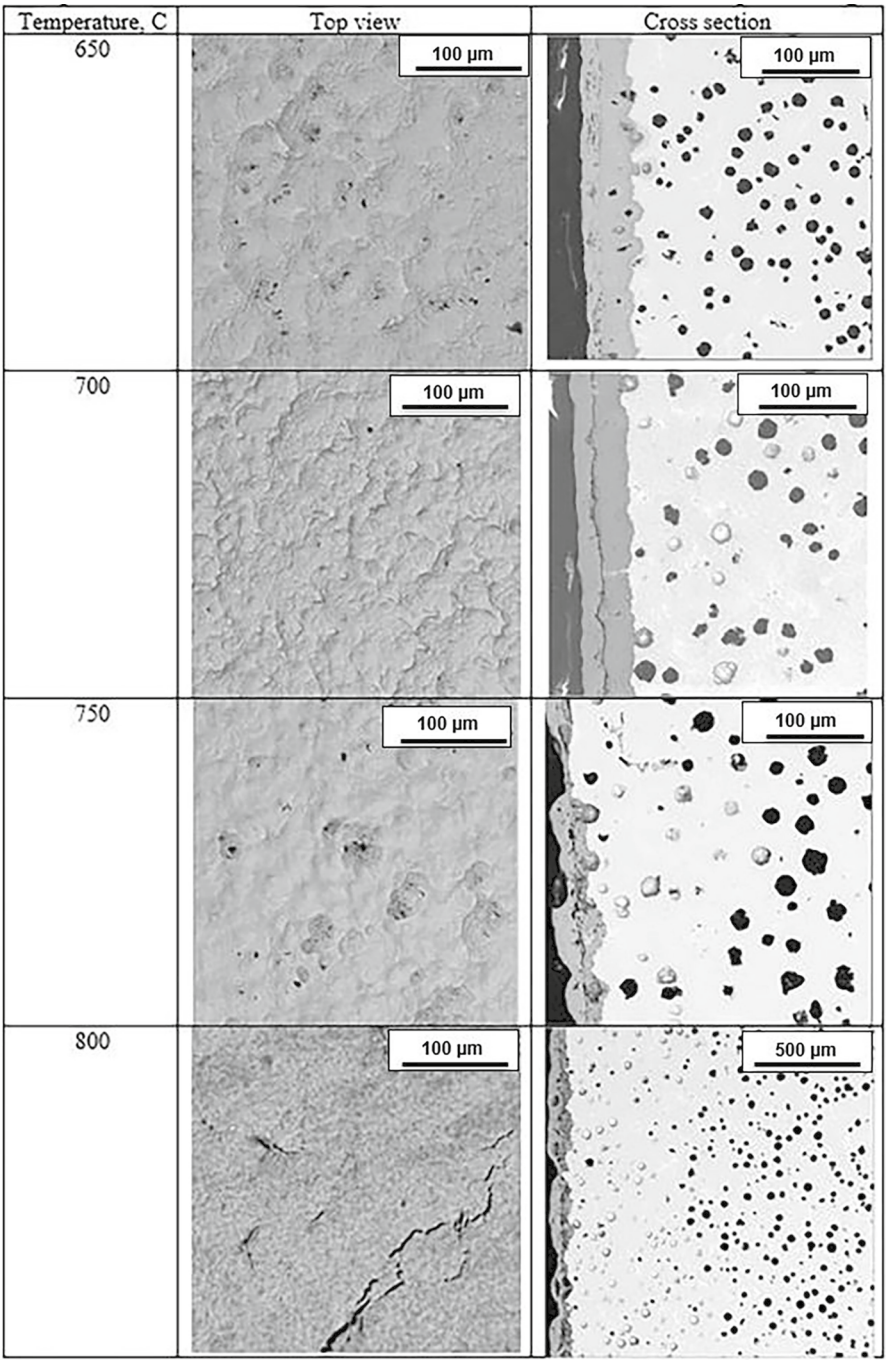

Fig. 7 Top view and cross sections of *SiMo* ductile iron oxidized in air during 100 h

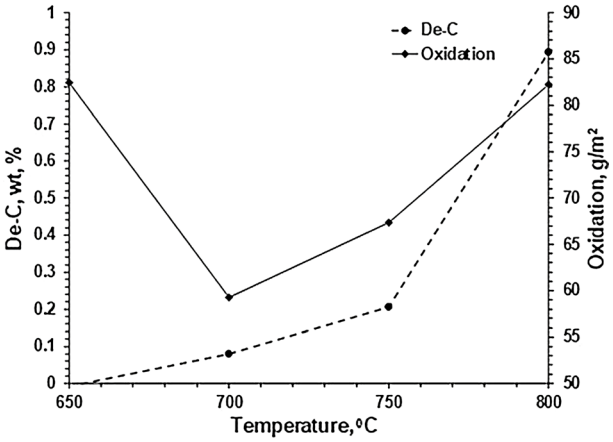

Fig. 8 De-*C* and true oxidation of *SiMo* ductile iron heated in air during100 h at different temperatures

was shown that the total weight change during the high-temperature exposure was related to weight gain due to oxidation and weight loss due to de-*C*. The applied methodology allowed these two processes to be differentiated. The importance of such adjustments of the original weight gain is illustrated in Fig. 9. The de-*C* had minor effect on the calculated true oxidation kinetics below 700 °C; however, at higher temperature, the total weight gain results required significant adjustment to achieve the true oxidation results because of the weight loss due to de-*C*.

There are several possible methods to decipher the data based on measured de-*C* from Leco C analysis or from measured de-*C* layer in cross section. In this study, de-*C* was estimated by carbon analysis and compared to measured thickness of de-*C* layer. Both methods require assumptions for recalculation of experimental data and

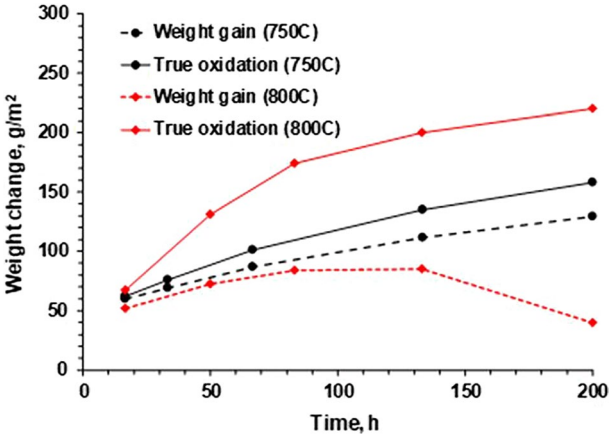

Fig. 9 Effect of adjustment of measured weight gain by weight loss due de-*C* to obtain the true oxidation rate (combustion atmosphere)

these assumptions were described in the Procedures. The change in *C* percent, or measured thickness of the de-*C* layer both need recalculations to account for the overall specimen weight loss, which can involve some experimental error. For example, there is no well-defined boundary between the de-*C* layer and the initial matrix in cast iron with spherical graphite. The SEM measurements of de-*C* layer were done in 5 places and standard deviation was reported. The Leco carbon analysis also was repeated using several samples which were cut from oxidized specimens. The correlation between a measured thickness of the de-*C* layer and a recalculated thickness from carbon combustion analysis is shown in Fig. 10. In this study, data from Leco carbon analysis was used to adjust the weight gain data and provide what it referred to as a "true" oxidation rate.

The coupled processes of de-*C* and surface oxidation could be qualitatively predicted from thermodynamic simulations, which used the local equilibrium concept at different ratios of added gas oxidant to *SiMo* ductile iron. The local equilibrium showed the conditions on different depths from the external surface of the specimen. In the graph shown in Fig. 11, the sum for all formed oxide phases was assumed to be equal to unity at each oxygen/alloy ratio. At restricted oxygen accessibility which relates a low ratio, graphite will be oxidized by forming a *CO* gas phase, and also a protection silica phase will be formed at metal/scale interface. The following internal layer will be developed as a mixture of fayalite with wüstite, and an external layer will consist of pure iron oxides. These calculations predict the sequence of formed layers, which were observed on the real scale formed in oxidized *SiMo* cast iron (Fig. 6 and Table 3).

A degree of de-*C* can be approximated by a power-law (Eq. 1):

$$\Delta C = k\tau^n \tag{1}$$

where: k and n are kinetics constants and τ is the time.

The experimental kinetics constant n at each temperature was determined by plotting $\mathrm{Ln}(\Delta C)$ versus $\mathrm{Ln}(\tau)$ (Fig. 12a). The slope values (n) were between 0.64 and 1.1 which are above the value 0.5 for the typical diffusion-control kinetics. The

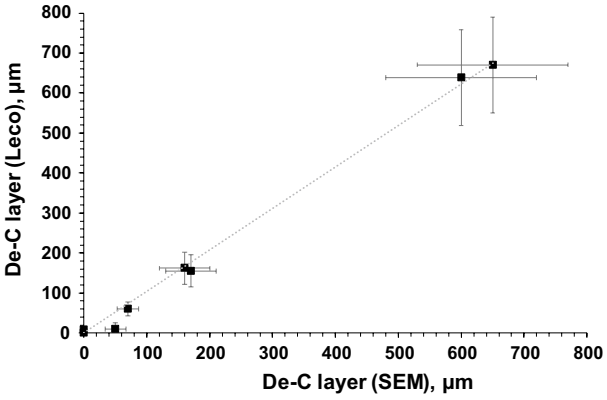

Fig. 10 Correlation between measured thickness of de-*C* layer and calculated from Leco *C* analysis

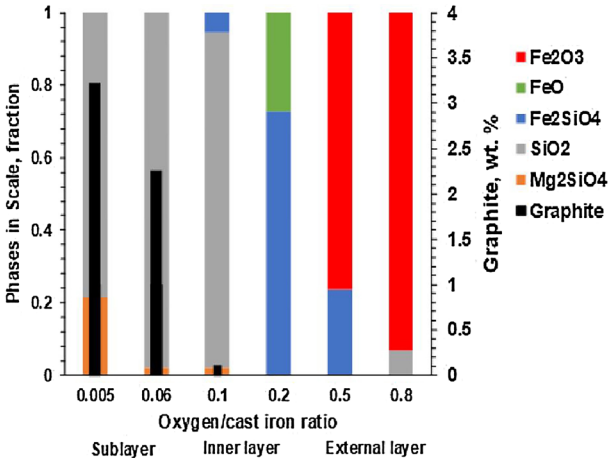

Fig. 11 Thermodynamic prediction of oxidation and de-*C* sequences of *SiMo* ductile iron at 800 °C

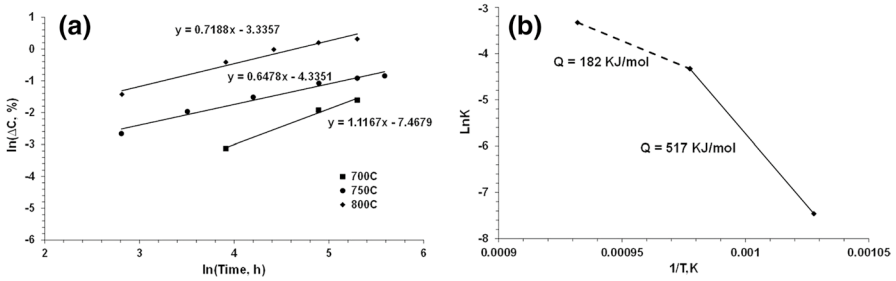

Fig. 12 *Ln(L)* versus *Ln(τ)* at different temperatures (**a**) and Arrhenius plot (**b**) for de-*C* of *SiMo* cast iron with spherical graphite oxidized in combustion atmosphere

intercepts of the plots corresponding to Ln*(k)* were plotted again at each reciprocal absolute temperature *T* (Fig. 12b) to obtain activation energy *Q* using Arrhenius Eq. 2:

$$\mathrm{Ln}(K) = \mathrm{Ln}\left(k_o\right) - Q/RT \tag{2}$$

where: k_0 is the constant, *R* is the gas constant.

The determined activation energy of de-*C* in *SiMo* ductile iron was 182 kJ/mol at temperatures above 750 °C. This value is higher than 125 kJ/mol activation energy of carbon diffusion in 3.6% *Si* alloyed ferrite [24] and close to 185 kJ/mol activation energy which was found during de-*C* of carbon steel at austenite stability temperatures [25]. However, the apparent activation energy of at temperature below 750 °C was unusually higher, which indicated interference with the other rate-controlling mechanisms. It could be assumed that increasing temperature destroyed the protective function of silica film on the metal/scale interface. To verify effect of silica film barrier, simplified estimation of de-*C* layer was done assuming that this process is

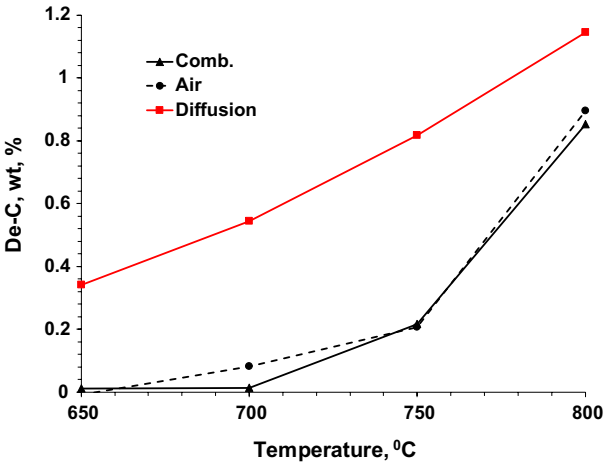

Fig. 13 Comparison of experimental de-*C* of *SiMo* cast iron during 100 h in air and combustion atmosphere with diffusion model for experimental test conditions

limited only by carbon mobility in the matrix. Figure 13 illustrates large differences between simulated de-*C* of used test specimen considering only carbon diffusion in ferrite (Eq. 3 [26]), and that was experimentally measured by carbon Leco combustion analysis of *SiMo* ductile iron oxidized in combustion atmosphere during 100 h:

$$C_x = C_0 \mathrm{erf}\left[0.5L/\left(D_c\tau\right)^{0.5}\right] \tag{3}$$

where: C_x in the carbon concentration in alloy at distance L, D_c is carbon diffusion coefficient, τ is time, and erf is the Gauss error function.

The deviation of the experimentally observed values n, activation energy, and carbon loss from the simplified model of diffusion-controlled de-*C* could be affected by an alloying element interference, barriers to the diffusion carbon from graphite nodules to the matrix, and diffusion resistance of formed oxides at the alloy/scale boundary. It was shown that cast structure significantly affects alloy de-*C* [18]. In spheroidal graphite cast iron, the graphite phase presented in the ferrite matrix as localized nodules. In such a structure, the de-*C* process and formation of porosity is controlled by transferring carbon through the graphite matrix boundary as well as bulk diffusion in the matrix. Cast iron with spherical graphite has a slower de-*C* rate when compared to oxidation of cast iron with compacted and flake graphite. Roles of these factors are more important at the lowest test temperature of 650 °C, and these barriers became less effective at 750–800 °C (Fig. 13). More investigations needed to be performed to verify interactions of different mechanisms.

Exhaust-side of exhaust manifolds exposes to combustion atmosphere containing water vapor, while air-side surfaces are oxidized in less humid air. It is well known that water vapor accelerates the oxidation reaction rate. Decoupling oxidation of alloy from de-*C* showed that these two processes are uniquely sensitive to the test atmospheres and temperatures. De-*C* intensified with increasing test temperature,

while the atmosphere showed minor differences (Fig. 13). On the contrary, the true oxidation was twice as intense in the combustion atmosphere, which contained water vapor (Fig. 14). Complicated temperature trends of the true oxidation rate indicated possible mutual effects. For example, at lower test temperatures, de-*C* could slow oxidation of other elements in an alloy by consuming oxygen; however, at higher temperatures, intensive de-*C* could promote oxygen penetration through developed porosity. Developed *CO* gas pressure could deform the surface of alloy and increase defectiveness of formed brittle protection silica film, which can cause cracks and voids in internal and external scale layers. These defects were observed on a scale formed at 800 °C in the combustion atmosphere (Fig. 6).

Both processes, including oxidation of the main alloy components and de-*C* of graphite nodules resulted in surface degradation of *SiMo* cast iron during service. The role of de-*C* could be disregarded below 700 °C, and this temperature could be considered a safe temperature for service. However, increasing temperature intensified the surface degradation by combining several mechanisms, which can increase surface defects. The comparison of surface degradation in the studied manifold with laboratory oxidation results suggests that this manifold was exposed during service to up to 700 °C temperatures because de-*C* and severe oxidation were identified along the exhaust and air sides; however, for full comparison exposure time and thermal stress also needed to be considered.

Conclusions

Surface and subsurface degradation of *SiMo* ductile iron during high temperature exposure in air and water vapor containing combustion gas atmosphere are related to complex effects of oxidation and de-*C*. The surface degradation during laboratory tests suggested that the in-service manifold was exposed to temperatures > 700 °C

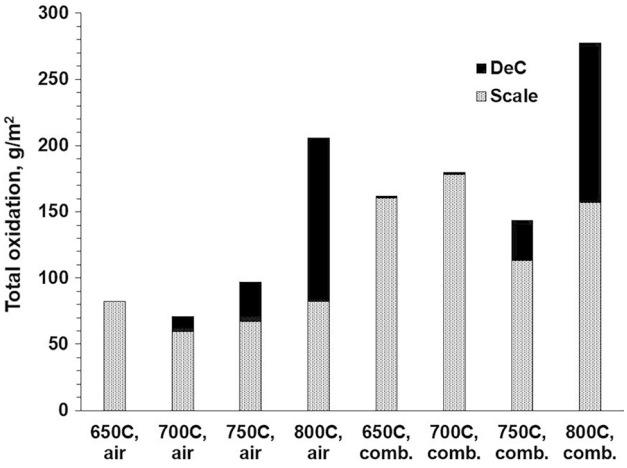

Fig. 14 Oxidation and de-*C* of *SiMo* ductile iron in air and combustion atmosphere (100 h test time)

as de-*C* and severe oxidation was identified along the inner and outer manifold surfaces.

The true kinetics of both the oxidation and de-*C* processes were established using experimentally measured weight gain and calculated weight loss due to de-*C*. It was shown that the rate of oxidation and de-*C* of *SiMo* cast iron with spherical graphite have different sensitivities to test temperatures and the specific conditions of the oxidizing atmosphere. At 700 °C and above, there are several significant mutual effects between scale formation and de-*C* processes which affect the kinetics of these processes.

The mutual effect of oxidation and de-*C* complicated the theoretical analysis of surface degradation in *SiMo* cast iron with spherical graphite. In both processes, atomic mobility of gas oxidant and alloy components play important roles, and simplified individual models for oxidation and de-*C* could be built assuming independence. However, complex analysis of the mutual effect of formation of multi-layered structure with silica protection barrier on metal/scale boundary, internal and external scale defects (cracks, lamination and spalling), pores in matrix from oxidized graphite nodules, and development of internal *CO* gas pressure will require sophisticated analytical models to account for all of these interactions. The experimental methodology for decoupling these processes will provide experimental data needed for future simulations.

Acknowledgements This material is based upon work supported by the U.S. Department of Energy's Office of Energy Efficiency and Renewable Energy (EERE) under the Award No. DE-EE0008458. Experimental tests were supported by the Peaslee Steel Research Manufacturing Center at Missouri S&T.

References

1. S. Park et al., Development of a Heat Resistant Cast Iron Alloy for Engine Exhaust Manifolds, SAE Technical Paper Series, SAE International, Technical Paper 2005-01-1688 (2005).
2. F. Tholence, and M. Norell, High Temperature Corrosion of Cast Alloys in Exhaust Environments I-Ductile Cast Irons. *Oxidation of Metals* **69**(1–2), 2007 (13–36).
3. M. Ibrahim, A. Nofal, and M. Mourad, Microstructure and Hot Oxidation Resistance of SiMo Ductile Cast Irons Containing Si-Mo-Al. *Met. Mater. Trans. B* **2**, 2017 (1149–1157).
4. M. Brady, et al., Long-term oxidation of candidate cast iron and stainless steel exhaust system alloys from 650 to 800 °C in Air with Water Vapor. *Oxidation of Metals* **82**(5–6), 2014 (359–381).
5. S. Lekakh, et al., Prevention of High-Temperature Surface Degradation in SiMo Cast Irons by Cr and Al Alloying. *Met. Mater. Trans. B* **51B**, 2020 (2542–2554).
6. N. Scheidhauer, C. Dommaschk, and G. Wolf, Oxidation Resistant Cast Iron for High Temperature Application. *Materials Science Forum* **925**, 2018 (393–399).
7. A. Ebel1et al., High-Temperature Oxidation of a High Silicon SiMo Spheroidal Cast Iron in Air with In Situ Change in H2O Content. *Materials Science Forum* **925**, 2018 (353–360).
8. S. Xiang, B. Zhu, and S. Jonsson, High-Temperature Corrosion-Fatigue Behavior of Ductile Cast Irons for Exhaust Manifolds. *Materials Science Forum* **925**, 2018 (369–376).
9. M. Ekström, P. Szakálos, and S. Jonsson, Influence of Cr and Ni on High-Temperature Corrosion Behavior of Ferritic Ductile Cast Iron in Air and Exhaust Gases. *Oxidation of Metals* **80**, 2013 (455–466).
10. M. Ekström, *Doctoral dissertation Oxidation and corrosion fatigue aspects of cast exhaust manifolds*, (KTH Royal Institute of Technology, Stockholm, 2015).
11. J. Dossett, and G.E. Totten *Steel Heat Treating Fundamentals and Processes*, ASM, 2013 vol. 4A.

12. Y. Chen, X. Xu, and Y. Liu, Decarburization of 60Si2MnA in Atmospheres Containing Different Levels of Oxygen, Water Vapour and Carbon Dioxide at 700–1000 °C. *Oxidation of Metals* **93**, 2020 (105–129).
13. Y. Chen, F. Zhang, and Y. Liu, Decarburization of 60Si2MnA in 20 Pct H2O–N2 at 700 °C to 900 °C. *Met. Mater. Trans. A* **51A**, 2020 (1808–1821).
14. J.-O. Park, T. Van Long, and Y. Sasaki, Feasibility of Solid-state Steelmaking from Cast Iron. *ISIJ international* **52**, 2012 (26–34).
15. S. Deng, and Y. Deng, *Advanced Materials Research* 1181–1185 (Trans Tech Publ, 2013).
16. E. Sharif-Sanavi and M. Mirjalili, A New Approach in Solid State Steelmaking from Thin Cast Iron Sheets through Decarburization in CaCO3 Pack, *ISIJ International* **58**, 2018 (1791–1800).
17. W. Lee, et al., Solid state steelmaking by decarburisation of rapidly solidified high carbon iron sheet. *Ironmaking & Steelmaking* **39**, 2012 (530–534).
18. Y. Yamaguchi, et al., Effect of graphite morphology on decarburized cast iron. *International Journal of Cast Metals Research* **16**, 2003 (137–142).
19. S. Lekakh et al., *Oxidation of Metals* **94**, 2020 (251–264).
20. R. Neu, and H. Sehitoglu, Thermomechanical fatigue, oxidation, and creep, Part 1. *Metallurgical Trans. A* **20A**, 1989 (1755–1767).
21. S. Méndez et al., Effect of Silicon and Graphite Degeneration on High-Temperature Oxidation of Ductile Cast Irons in Open Air. *Oxid. Of Metals, Oxid. Met.* **91**, 2019 (225–242).
22. FactSage Thermochemical Software, www.factsage.com.
23. A. Kurbet, S. Dubey, A. Kumar, and S. Razdan, Design and Analysis of an Exhaust Manifold Subjected to Thermo-Mechanical Loading. *International Engineering Research Journal (IERJ). Special Issue* **2**, 2015 (4494–4503).
24. A. Vasilyev and P. Golikov, Carbon diffusion coefficient in alloyed ferrite. *Materials Physics and Mechanics* **39**, 2018 (111–119).
25. S. Valette, A. Denoirjean, D. Tétard, and P. Lefort, C40E steel oxidation under CO2: Kinetics and reactional mechanism. *Journal of alloys and compounds* **413**, 2006 (222–231).
26. D. Porter, K. Easterling, Phase Transformations in Metals and Alloys, 2nd ed.; Chapman & Hall: London, UK, 1992; pp.74.